Received 18 October 2024; revised 13 November 2024; accepted 19 November 2024. Date of publication 25 November 2024; date of current version 11 June 2026.

Digital Object Identifier 10.1109/OJAP.2024.3505424

Reflectarray 2-D Beam-Steering With Graphene on Copper Elements for 6G Point-to-Point Communication

SUHAIL ASGHAR QURESHI [1], MUHAMMAD RAMLEE KAMARUDIN [1] (Senior Member, IEEE), YOSHIHIDE YAMADA [2] (Senior Member, IEEE), MUHAMMAD INAM ABBASI [3] (Senior Member, IEEE), MUHAMMAD HASHIM DAHRI [4] (Member, IEEE), ZUHAIRIAH ZAINAL ABIDIN [1] (Senior Member, IEEE), AND NORDIN RAMLI [5] (Senior Member, IEEE)

[1] Faculty of Electrical and Electronic Engineering, Universiti Tun Hussein Onn Malaysia, Batu Pahat 86400, Malaysia
[2] Malaysia Japan International Institute of Technology, Universiti Teknologi Malaysia Kuala Lumpur, Kuala Lumpur 54100, Malaysia
[3] Faculty of Electrical and Electronic Engineering Technology, Universiti Teknikal Malaysia Melaka, Durian Tunggal 76100, Malaysia
[4] Department of Telecommunication Engineering, Dawood University of Engineering and Technology, Karachi 74800, Sindh, Pakistan
[5] Wireless Innovation Department of Corporate Technology, MIMOS Berhad, Kuala Lumpur 57000, Malaysia

CORRESPONDING AUTHORS: MUHAMMAD RAMLEE KAMARUDIN and MUHAMMAD INAM ABBASI (e-mail: mramlee@uthm.edu.my; inamabbasi@utem.edu.my)

This work was supported by the Ministry of Higher Education (MOHE) through Fundamental Research Grant Scheme under Grant FRGS/1/2021/TK0/UTHM/02/19, and Communication of this research is made possible through monetary assistance by Universiti Tun Hussein Onn Malaysia (UTHM) and the UTHM Publisher's Office via Publication Fund E15216.

ABSTRACT This work presents a graphene-based Reconfigurable Reflectarray Antenna (RRA) for 6G point-to-point communications. Unlike the conventional dimensions of less than λ/8 to act as the main resonant element, Graphene has been designed at λ/2 dimensions, which works as the phase-shifting element under a copper patch. Graphene's chemical potential can be varied by applying DC biasing to array elements so that the reflection coefficient phase of the unit cells can be adjusted to form a collimated beam in a certain direction. An array of 977 elements with an aperture diameter of 15λ produced a collimated beam through two states of DC biasing to graphene, i.e., "On" and "Off". Later, the beam steering performance of the designed RRA was analysed in the E-plane and H-plane. Furthermore, the effect of the focal length to diameter ratio (F/D) is also evaluated on the highest gain and the steering range. The highest gain of 25.6 dBi was obtained at 125 GHz with a beam steering range of ±30° with a gain loss of 3 dB when the F/D ratio was 0.9. However, the best beam steering range of ±45° with a gain loss of 3 dB was obtained when the F/D ratio was 1.1 and the highest gain of 23.25 dBi. Overall, the aperture efficiency was found to be 13% which is sufficient compared to conventional phase shifters at high frequencies. The 1-dB gain of the designed array was found to be 8.8%, 7.2% and 6.4% in the case of F/D ratio of 1.1, 1.0 and 0.9, respectively. Owing to the broadband operation from 122 GHz to 128 GHz, beam steering range, and aperture efficiency, the designed RRA shows the potential to be incorporated with reconfigurable intelligent surface (RIS)-based communications for 6G point-to-point communications.

INDEX TERMS 6G, beam-steering, graphene, RRA.

I. INTRODUCTION

POINT-TO-POINT (P2P) communication has been practised as a solution to the demand for increased backbone link transmission rate and accompanying limitation factors. The transmission and exchange of data are strongly influenced by the drastic surge in the first and last-mile transmission rate. Terahertz (THz) band offers up to 10 Gbps data transfer rate in theory for P2P communication [1]. Thus, the THz band also presents new requirements for antenna development. High-gain antennas are generally indispensable because of the THz band's intrinsic high path loss [2]. Moreover, antennas should be flexible and adjustable under communication conditions where the end user is expected to move so that a satisfying signal-to-noise ratio can be maintained. Reflectarray Antenna (RA) is a suitable candidate for the THz band in environments with dense multipath to offer single and multiple pairs of transmitter and receiver to communicate and extend transmission range simultaneously [3]. Owing to their low cost and flexibility, RAs are typically used for satellite communications, P2P links and radars [3]. Generally, RA is a flat reflector comprising multiple resonating elements with a ground. The reflection phase of each component is tuned to shape or collimate the radiation pattern when illuminated by a horn antenna [4]. The required change of reflection phase for each reflectarray unit cell can be acquired by changing the element's dimension, rotation or geometry [5]. Once a conventional RA has been designed, its radiation pattern remains fixed, and beamforming is restricted to a predetermined angle. This limitation underscores the significance of electronically tuneable unit cells, which enable the adjustment of the antenna elements. By employing such cells, it becomes possible to achieve electronic beamforming at various angles, enhancing the versatility and functionality of the antenna system. Electronically tuneable reflectarrays have been developed in microwave bands by embedding PIN diodes with elements [6], [7], [8], [9]. The unit cell's resonance frequency shifts to a higher or lower direction with the switching of PIN diode states depending on its configuration [10]. In contrast, a varactor diode can be used as a device to regular the overall capacitance of the unit cell by changing the bias voltage [11]. Similarly, liquid crystals (LCs) can also be controlled through voltage, whose permittivity changes with respect to the applied voltage [12]. However, diodes are difficult to integrate into the applications of frequencies larger than a millimetre-wave band. PIN diode was used recently for the millimetre-wave RRA [13]. The unit cell was designed with a couple of PIN diodes soldered at positions on a complementary ring. For fabrication, a combination of laser engraving techniques and printed circuit board (PCB) was used [13]. For higher frequencies, liquid crystals have been employed to design RRAs. The design, fabrication and measurements were conducted for an RRA based on LC operating at over 100 GHz. However, liquid crystal is bulky, and its large response time makes it complicated for high-frequency applications [14].

On the other hand, graphene is a type of material in which conductivity changes in thin atomic sheets with the application of bias voltage. In [15], a graphene-based reflectarray was proposed operating at over 1 THz frequencies. The size of each element was about $\lambda/16$ and the full array consisted of 25,000 elements. It was shown that the plasmonic propagation of graphene improves the performance of RA in terms of bandwidth and cross-polarization. A graphene-based RRA was proposed in [16] for the generation of vortex waves in the THz band. The unit cell was designed at $\lambda/16$ and the graphene patch's dimensions were $\lambda/24$. A reflective cell was examined to demonstrate that the reflection phase could be controlled by changing graphene's chemical potential. Similarly, a graphene-based metamaterial array was also proposed for the generation of OAM vortex waves in the transmitting mode [17]. A multilayer element was capable of 360° phase deviation in transmission coefficient with the change in graphene's chemical potential from 0 to 0.8 eV. The transmitarray was able to produce distinct tuneable modes of 0, ± 1 and ± 2 in wide band coverage of 4.2-5.6 THz. However, no RRA has been proposed so far for the application of beam steering using graphene as phase phase-shifting element.

In previously published works, graphene is used as the main patch/conducting element and its properties are controlled by applying different voltage levels [2], [18], [19], [20]. Moreover, it was necessary to design it at less than $\lambda/16$ dimensions due to the plasmonic nature of graphene so that it resonates, and its reflection coefficient phase can be altered. However, it makes it difficult to fabricate graphene at such small dimensions and embed it in the structure for applications such as array antennas and applying biasing voltage at the same time for distinct numbers of cells. In this manner, a potential solution is to use graphene at typical $\lambda/2$ dimensions in a reflectarray element, where graphene cannot resonate itself, but it can act as the phase-shifting element. Therefore, this article proposes the application of graphene as phase switching in a unit cell like that of a PIN diode or liquid crystal for designing RRA for beam steering at over 85 GHz. The unit cell is designed at approximately $\lambda/2$ dimensions and a graphene-metal hybrid structure is used to resonate the element.

II. METHOD

A. MODELLING OF GRAPHENE

Graphene is a single atomic-layered microscopic material. It has electric and optical properties such as high carrier mobility and zero band gap structure [21]. The electrons in graphene are affected by interaction with high-frequency waves, which alters its electrical conductivity. This property of graphene makes it extraordinary to use for THz wireless communications. Graphene can be employed for various applications [22]. When high-frequency waves come into contact with graphene, they affect how these electrons behave, leading to alterations in electrical conductivity that can be gauged accurately. This quality makes graphene a perfect choice for THz detectors, allowing the creation of super-sensitive sensors that can pick up even the slightest THz signals [23]. Graphene offers exciting possibilities for various uses such as sensing, gas absorption, energy storage and other electronic applications etc. [24]. In super-fast wireless communication, using graphene can completely change how data is sent providing lightning-fast speeds and much more space for information [25]. This is not just important for making the current wireless systems better, but it also opens the door for new and creative ideas like

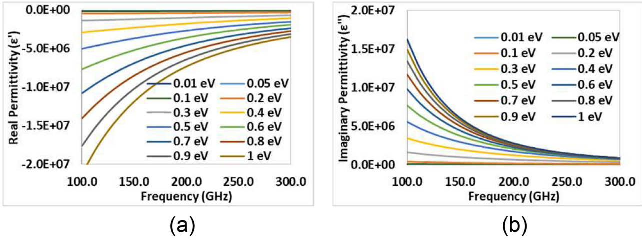

FIGURE 1. **(a) Real and (b) Imaginary Permittivity of Graphene.**

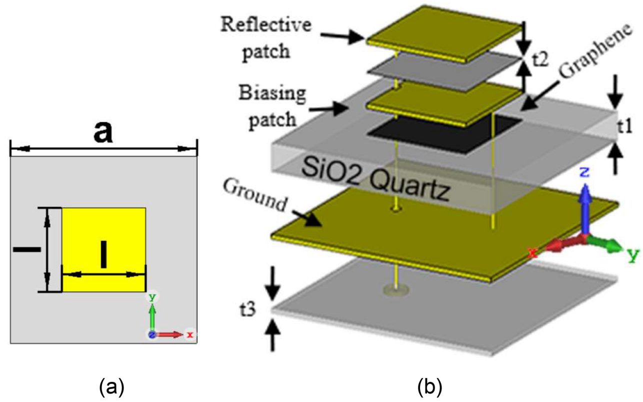

FIGURE 2. **Unit cell design (a) top view and (b) perspective 3D view of biasing mechanism.**

super-fast Internet and watching super clear videos in real-time [25]. The conductivity of graphene can be changed by varying the biasing voltage. This is possible due to the dependence of graphene's conductivity on chemical potential as given by (1) [26].

$$\sigma_g = \frac{2e^2 k_B T}{\pi \hbar^2 (\omega + i\tau^{-1})} \ln\left(2\cosh\left(\frac{\mu_c}{2k_B T}\right)\right) \tag{1}$$

Here, k_B represents Boltzmann's constant (eV/K), T is temperature (K), ħ is reduced Plank's constant (Js), e is the electron charge (statcoulombs), μ_c denotes chemical potential (eV), τ denotes free-electron relaxation time (s), vf is the fermi velocity with a reported value of 1.2×10^6 m/s [27] and μ_n is electron mobility with the reported value of 30,000 cm^2/V.s for unsuspended graphene [28]. It was also reported that the relaxation time (τ) depends on chemical potential (μ_c) as represented by (2).

$$\tau = \left|\frac{\mu_c \mu_n}{v_f^2}\right| \tag{2}$$

By inserting the value of μ_n and vf^2, (2) can be simplified as follows:

$$\tau = 2.08 \times \mu_c \times 10^{-12} \tag{3}$$

The relative permittivity of graphene can be described in the form of conductivity as follows:

$$\varepsilon_g = 1 + \frac{i\sigma_g}{\omega\varepsilon_0\Delta_g} \tag{4}$$

The conductivity of the graphene sheet is changed dynamically by the application of bias voltage [29]. The top-gate configuration of graphene's biasing leads to a change in the chemical potential of graphene, which can freely modulate between 0.01 eV and 1.0 eV [30]. The complex permittivity of 2D layer graphene from 100 to 3000 GHz is represented in Fig. 1.

The Fermi energy of graphene, which is also known as graphene's chemical potential can be controlled via applied voltage as described by (5) [31]:

$$V = V_0 + \frac{te\mu_c^2}{\varepsilon_0\varepsilon_r\pi\hbar^2 V_f^2} \tag{5}$$

V_0 represents the voltage related to internal chemical potential (which is negligible), V is the DC biasing applied, t is the thickness of the substrate, relative permittivity is represented by ε_r, ε_0 is free-space permittivity and Fermi velocity is represented by V_f.

B. REFLECTARRAY ELEMENT

The proposed reflectarray (RA) element consists of multiple layers in a typical shape of a rectangle unit cell patch backed by ground plane as depicted in Fig. 2. The Copper layer serves the main purpose of resonance, which follows the dielectric spacer and the biasing layer of copper to apply biasing the graphene 2D layer between the substrate in order to achieve reconfigurability. The quartz substrate with a dielectric constant (ε) of 3.75 and tangent loss of 0.0004 is used due to its greater compatibility with graphene sheets compared to other substrates [32]. The lattice constant (a) of the unit cell was 1×1 mm^2. The length and width were the same, represented by 'l' in Fig. 2(a), with the dimensions of 0.45 mm. The thickness of the substrate (t1) was 0.12 mm, and the thickness of copper was 0.018 mm. The thickness of dielectric spacer (t2) between the reflective patch and the biasing patch is 0.01 mm. Indeed, the resonance of the patch element of copper with graphene grown on it leads to shifting of resonance towards higher frequencies due to the decrease in the graphene's permittivity, subsequently enabling the reconfigurability of the reflection coefficient phase with the control of graphene's biasing voltage. The biasing technique of graphene is represented in Fig. 2(b) in a layered view. The biasing patch is connected to the ground line, while the reflective patch is connected to the vias. The reflective patch is isolated from the biasing patch, graphene and ground. Utilising (5), the requisite external direct current (DC) bias voltage for the reconfigurable graphene-based terahertz (THz) microstrip patch is determined to be 24 V. This calculation is based on a dielectric spacer thickness of 10 nm (t2) with a relative permittivity (ε_r) of 3.75. The thickness of the bottom substrate (t3) below ground is 0.025 mm. The unit cell was simulated under boundary conditions in which the electric field was aligned along the y-axis, while the magnetic field was aligned along the x-axis.

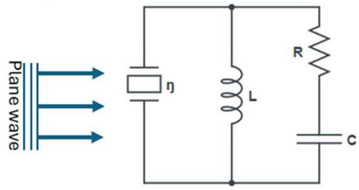

FIGURE 3. Equivalent circuit for the unit cell.

TABLE 1. R-L-C equivalent circuit values.

State	μ_c (eV)	R (Ω)	L (pH)	C (pF)
Off	0.01	17.2	0.156	0.0142
On	1.0	1.19	0.06	0.0211

The FEM technique was used to simulate the reflection coefficient of the unit cell with boundary conditions shown above with the help of CST Studio. To simplify the configuration of reflectarray and to avoid using many variables, only two states of chemical potential were used, i.e., 0.01 eV and 1.0 eV. The condition of 0.01 eV on graphene can be imagined as the state with no supply of biasing, while chemical potential reaches 1.0 when voltage is applied to graphene. In this manner, the proposed reflectarray can be supposed as a 1-bit reconfigurable reflectarray, in which diodes are typically used for "On" and "Off" states [33], [34], [35]. Therefore, graphene's Fermi energy of 0.01 eV will be referred to as the "Off" state and 1.0 eV will be referred to as the "On" state in this paper. The equivalent physical circuit of the proposed unit cell can be modelled with equivalent R-L-C components as shown in Fig. 3, where η represents impedance characteristics of free space [36]. The values of R-L-C components were tuned using the Advanced Design System (ADS). The extracted values are shown in Table 1 for both the "On" and "Off" states of graphene's biasing. It can be observed that the resistance decreases in the "On" state, which is perfectly explained by the fact that the rise in the chemical potential of graphene increases the conductivity of graphene. The reflection coefficient magnitude and phase response of the unit cell on two different states are shown in Fig. 4. Fig. 4 also compares the reflection coefficients obtained by the equivalent circuit with the simulated results. An excellent matching has been observed in amplitude. It can be seen from Fig. 4(a) that the reflection coefficient at 125 GHz is 5 dB in the "Off" state and 0.7 dB in the "On" state. As shown in Fig. 4(b), the reflection coefficient phase is found to be $-50°$ at 125 GHz in the On state, corresponding to a dielectric permittivity of -1.6×10^7 and a tangent loss of 0.6 for graphene (according to Fig. 1 at 125 GHz). Conversely, when the permittivity of graphene is -2.1×10^2 and the tangent loss is 61 (according to Fig. 1 at 125 GHz), the reflection coefficient phase is recorded at $-270°$. Moreover, the reflection phase difference is over 180° from 112.5 GHz to 137 GHz, and it is maximum at 125 GHz. The greyed area represents the expected bandwidth of 1-bit RRA, which makes 19% according to the centre frequency of 125 GHz.

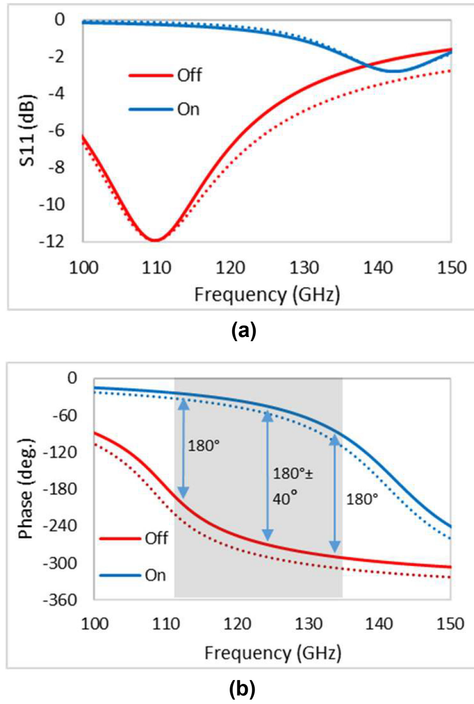

FIGURE 4. Comparison of simulated (---) and equivalent circuit (---) (a) reflection coefficient amplitude and (b) phase.

To obtain optimum results, a 1-bit reconfigurable reflectarray must have 180° of phase difference and reflection loss to be minimum in the operating frequency.

The rationale for integrating graphene with a copper patch, as previously discussed, is primarily based on the fact that graphene, due to its plasmonic characteristics, does not resonate at half-wavelength (λ/2) dimensions. As shown in Fig. 5(a), there is no resonance when biasing is applied to graphene. Subsequently, the phase difference required between the On and Off state at the desired frequency is not obtained without a patch as shown in Fig. 5(b). Although the phase difference is high at frequencies above 140 GHz, which can be brought to lower frequencies by adjusting the dimensions of the graphene element, however, it will tend to increase the phase difference as well that is above the margin of 1-bit quantisation (way more than 180±40 degrees). Fig. 6 depicts the electric field intensity on the surface of the unit cell for both states of 1-bit RRA. The direction of the E-field distribution reverses at 125 GHz when the Fermi energy of graphene is changed from 0.01 eV to 1.0 eV.

III. PHASE COMPENSATION AND RADIATION PATTERN

The planar reflectarray in essence is analogous to parabolic reflector [37]. However, reflectarray comprises a limited number of elements arranged in such a way that the phase distribution of the RA aperture is pixelated. The Electromagnetic (EM) waves originating from the feed (typically horn antenna), have spherical wave propagation. The incident EM waves on the aperture of RA have a phase corresponding to the separation between the feed and RA

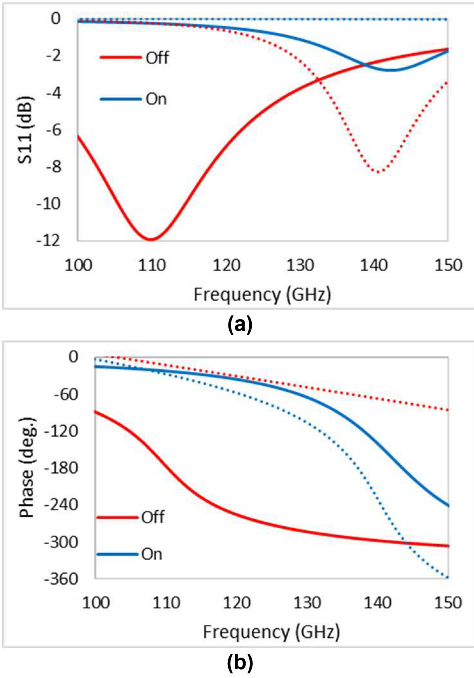

FIGURE 5. Comparison of simulated reflection coefficient with (---) and without patch (...) (a) reflection coefficient amplitude and (b) phase.

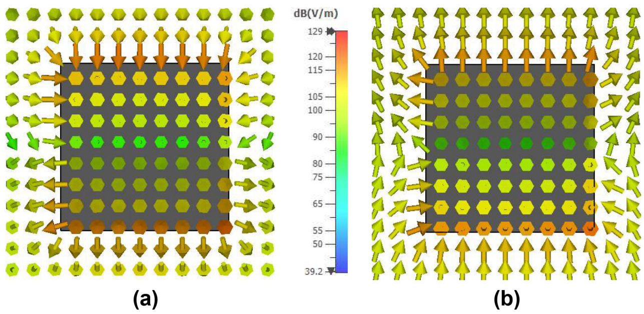

FIGURE 6. E-field (a) 0.01 eV and (b) 1.0 eV.

surface. Therefore, the elements on the RA aperture have to compensate for the distance travelled by incident EM waves, which is called spatial phase delay (Φ) [38]. In such a way, a collimated beam can be achieved. The reflecting phase of each unit cell on RA should compensate for the spatial phase delay from the feed centre to the specific unit cell. An array of 977 elements was modelled. The circular-shaped array has a diameter of 35 mm, which is about 15 times the wavelength at 125 GHz. Mathematically, phase compensation is defined by (6)–(7) [39].

$$\Phi(\theta, \varphi) = \frac{2\pi}{\lambda}(\mathrm{R_i} - \sin\theta(\mathrm{x_i}\cos\varphi + \mathrm{y_i}\sin\varphi)) \tag{6}$$

$$\mathrm{R_i} = \sqrt{(\mathrm{x_i} - \mathrm{x_f})^2 + (\mathrm{y_i} - \mathrm{y_f})^2 + (\mathrm{z_i} - \mathrm{z_f})^2} \tag{7}$$

$\Phi(\theta, \varphi)$ is the direction of the reflection beam where θ and φ are the reflection angles in the horizontal and vertical plane, respectively. $\mathrm{x_i}$, $\mathrm{y_i}$, $\mathrm{z_i}$ are the coordinates of the certain unit cell on reflectarray, while $\mathrm{x_f}$, $\mathrm{y_f}$ and $\mathrm{z_f}$ are the

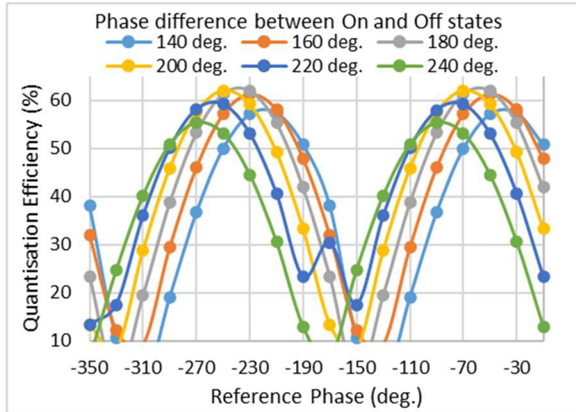

FIGURE 7. Calculated quantisation efficiency versus reference phase for varying phase differences.

coordinates of the phase centre of the feed antenna. Since this is designed as a 1-bit RRA, the phase compensation must be quantised. The quantised phase response required is given in (8).

$$\Phi = \begin{cases} -50^\circ, & 1.0\ \text{eV} \quad \Phi > -180^\circ \\ -270^\circ, & 0.01\ \text{eV} \quad \Phi < -180^\circ \end{cases} \tag{8}$$

where, Φ is the required phase of each reflectarray element, which is quantised to only two states, i.e., -50° or -270°. Since the required phase is quantised, the aperture efficiency is reduced due to quantisation error. By carefully selecting the right phase values for the On and Off states, it is possible to minimise the effect of 1-bit quantisation error. The quantisation efficiency can be calculated with the help of the array factor using (9) [10].

$$\eta_{\mathrm{q}} = \frac{\left|\mathrm{AF}(\theta, \varphi)_{1-\mathrm{bit}}\right|^2}{\left|\mathrm{AF}(\theta, \varphi)_{\mathrm{continuous}}\right|^2} \tag{9}$$

where $\mathrm{AF}(\theta,\ \varphi)_{\text{1-bit}}$ is the array factor considering the 1-bit quantisation whereas $\mathrm{AF}(\theta,\ \varphi)_{\mathrm{continuous}}$ is the array factor considering the continuous progressive phase. The quantization efficiency is illustrated in Fig. 7 for varying phase differences between the On and Off states across different reference phases. The quantisation efficiency in this study was found to be 58% for the reference phase of -270° and the phase difference of 220°.

A schematic of the designed RRA system, representing the position of the feed and the RRA is given in Fig. 8(a). Phase distribution of the incident (feed antenna) electric field on the reflectarray plane was calculated using (6), which is depicted in Fig. 8(b). Fig. 8(a) also shows the electronic beam steering mechanism of RRA, which must consist of a microcontroller unit and the voltage distribution controller (FPGA). The voltage distribution controller should contain 10 inputs so that combinations of On and Off output configurations are 1024, which is higher than the number of elements in the designed array. Based on the phase distribution obtained, a reflectarray can also be realised

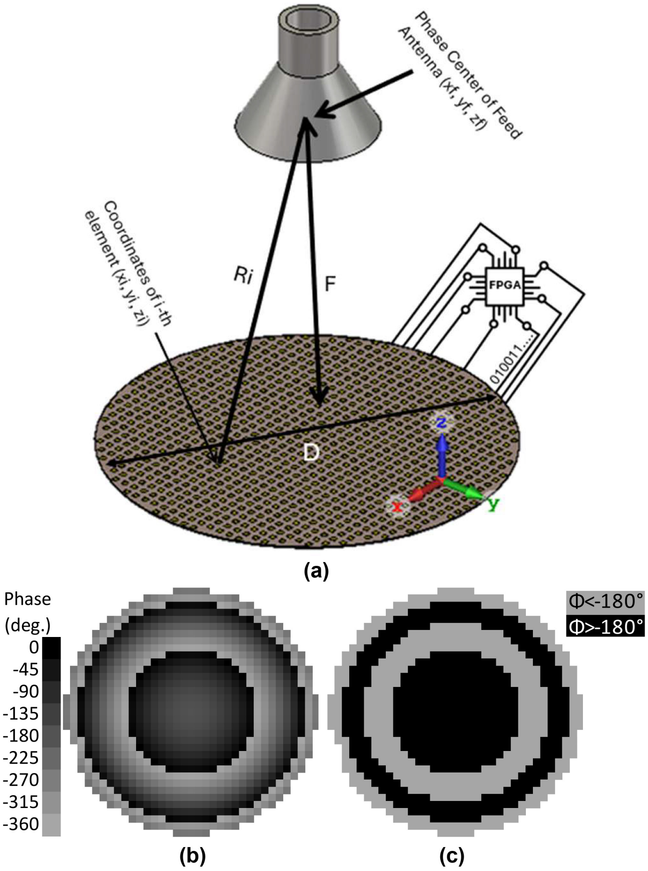

FIGURE 8. (a) Layout of the proposed centre-fed RRA with the conical horn antenna, (b) Calculated phase distribution of the incident electric field of feed antenna on the reflectarray plane and (c) its 1-bit quantisation.

by the proposed graphene-assisted unit cells with only two states of biasing. Using the approximation in (8), the required quantised phase distribution of the RA elements is represented in Fig. 8(c).

It is well noted that the phase distribution of the reflectarray antenna depends on the distance of the feed antenna from the reflective plane (F), and frequency of operation, while the aperture efficiency of the antenna depends on the distance (F), size of antenna (D), and radiation beam of feeding source, typically characterised by $\cos^{q}(\theta)$ [40], where q is determined using (10) [41].

$$q = \frac{-0.15}{\log\left[\cos\frac{\theta}{2}\right]} \tag{10}$$

The feeding source for the RA was designed to complete the RA mechanism, whose dimensions and radiation pattern are shown in Fig. 9. The designed feed antenna is a conical horn antenna whose horn radius (r_1) is 5.25 mm, waveguide radius (r_2) is 1.85 mm, the horn length (d_1) is 6 mm, and the waveguide length (d_2) is 4.11 mm. The thickness of the horn is 0.65 mm. It can be seen from the radiation pattern that the normalised −10 dB gain in both the E-plane and H-plane appears at around 25°. Moreover, the −3 dB beamwidth

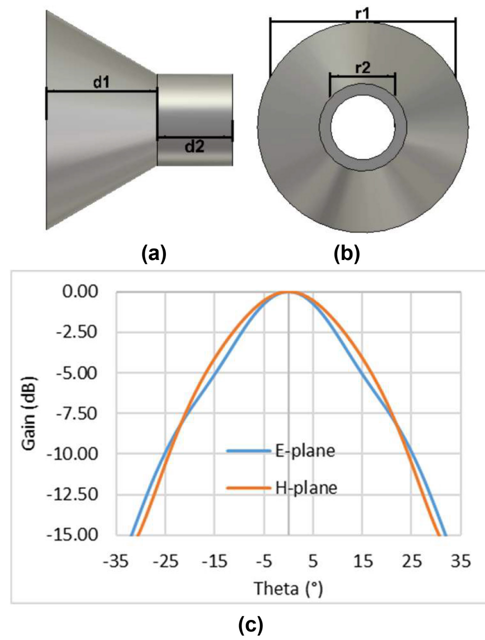

FIGURE 9. (a) side view of horn antenna, (b) back view of a horn antenna and (c) its simulated radiation pattern at 125 GHz.

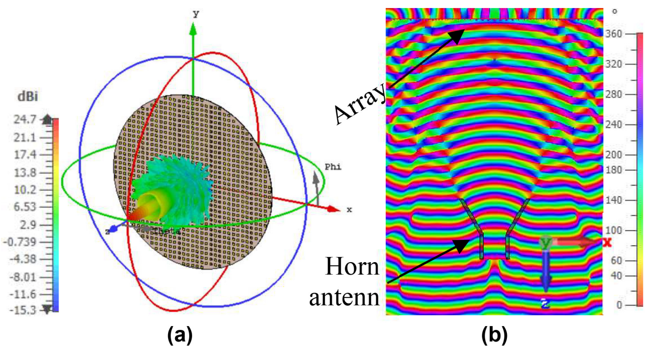

FIGURE 10. (a) Simulated 3D radiation pattern of a designed reflectarray antenna (b) Phase front along the z-axis of the reflected wave.

of the E-plane is 25.1°, while it is 21.2° in H-plane. The centrally fed method is adopted in this study in order to evaluate the performance of the proposed RRA antenna. For maximum aperture efficiency, it is recommended in theory that the array is illuminated by −10 dB gain of feed antenna on its edges [42]. To satisfy that condition, the distance from the feed centre to RA (F) is determined to be the same as the size of the antenna aperture (D), which is 35 mm. In other words, the ratio of F/D is equal to 1. In this way, the illuminated efficiency of RA is determined to be 77% and spillover efficiency is determined to be 94%.

The designed RA was simulated in the Finite Integral Method (FIT) method using CST Studio. The simulated 3D radiation pattern at 125 GHz is given in Fig. 10(a) with the main beam direction at $(\theta, \varphi) = (0°, 0°)$. The maximum gain obtained at 125 GHz is 24.7 dBi with side lobe levels less than −13 dB. The angular −3 dB beamwidth is 3.9° in E-plane and 4.1° in H-plane. The phase front pattern was

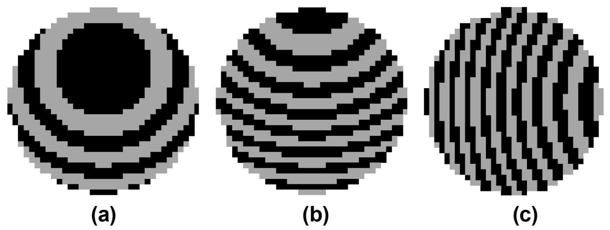

FIGURE 11. Calculated phase distribution on the reflectarray plane at 125 GHz for beam steering at (a) 10° in the H-plane, (b) 30° in the H-plane, (c) 40° in the E-plane (black pixel represents the "On" state while grey blocks represent the "Off" state of biasing.).

observed at a distance of 40 mm as shown in Fig. 10(b). However, the phase front pattern remains constant at any distance longer than the distance of the feed antenna from reflectarray. Since the array is centrally fed by the feed antenna, phase front distribution fluctuates at the centre up to the diameter of the horn antenna due to blockage losses. The change in phase front is almost linear elsewhere by the edges of the array. This validates the plane-wave configuration of the designed reflectarray.

IV. BEAM STEERING AND DISCUSSION

Later, the 2D beam steering mechanism is demonstrated by realising numerous collimated beams at certain directions in both the E-plane (Phi = 0°) and H-plane (Phi = 90°). The radiation patterns with main beam directions at theta ranging from 0° to 55° are simulated in E-plane and H-plane at 125 GHz. The functionality of 2D beam steering is exhibited by realising a collimated beam in two different planes at different angles. The reflection coefficient phase distributions required for steering the beam in different directions are obtained using (6). The angles of θ and φ define the direction of the steered beam. In the E-plane, φ is zero and θ was varied from 0° to 55°, while φ was varied and θ was kept zero in the H-plane. The "On" and "Off" states of graphene biasing for main beams at theta of 10° and 30° in the H-plane and 40° in the E-plane are represented in Fig. 11(a), 11(b) and 11(c), respectively. Since the reflection phase determined for above $-180°$ was $-50°$, which is obtained during the "On" state and the reflection phase determined for below $-180°$ was $-270°$ according to (8), which is "Off" state.

Fig. 12(a) represents the gain of steered collimated beams with their highest gain in the H-plane, while Fig. 12(b) represents the gain of the steered beams in the E-plane at the desired frequency of 125 GHz. The maximum gain reported at theta, 0° is 24.7 dBi, which is consistent up to the beam steering angle of 35° and starts to decline when the steering angle is more than 30°. This is evident from the highest gains found at 0°, 10°, 20° and 30°, which are 24.7 dBi, 23.9 dBi, 23.7 dBi and 23.8 dBi, respectively in E-plane. The maximum gains in the case of an E-plane for the same angles are 24.7 dBi, 23.8 dBi, 23.7 dBi and 23.4 dBi. However, the gain is found to be more than 20 dBi until a steering angle of 45°. The beam steering in the E-plane and H-plane is obtained up to ±45° with a 4 dB drop in gain. The lowest

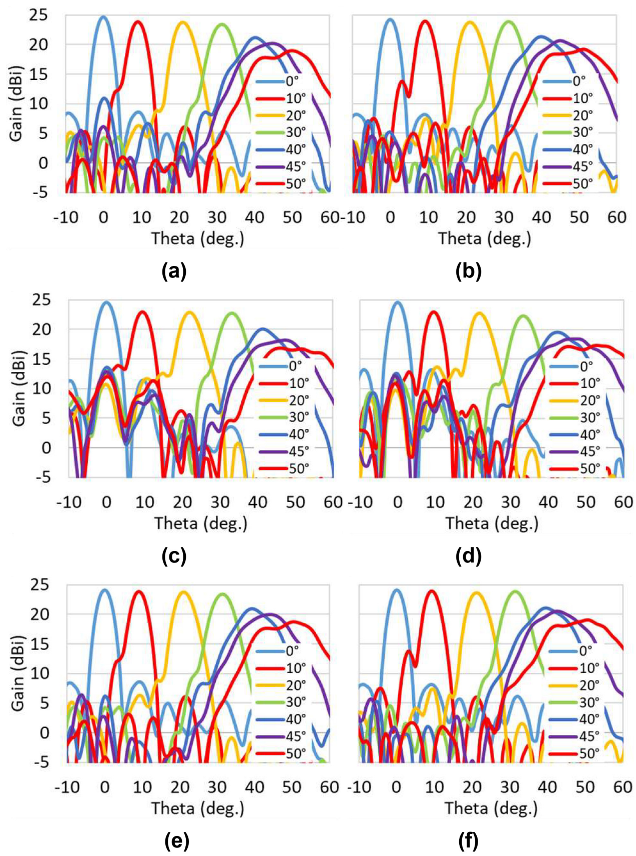

FIGURE 12. Simulated beam steering accomplished by the individual phase manipulation of array elements utilising full array simulations in (a) H-plane at 125 GHz, (b) E-plane at 125 GHz, (c) H-plane at 122 GHz, (d) E-plane at 122 GHz, (e) H-plane at 128 GHz and (f) E-plane at 128 GHz.

gain is indeed obtained in the case of the highest steered beam, which is 50° in this study where it is 19 dBi in the H-plane and 19.2 dBi in the E-plane. It can also be noted that the beams are not exactly pointing at 50° in both the E- and H-plane regardless of the configuration of RRA to generate a beam at 50°. This is due to the configuration of unit cells based on the prediction of reflection phase responses in full-wave simulation under ideal circumstances, i.e., illumination of normal incident plane waves and periodic arrangements of array elements. Fig. 12 also shows broadband characteristics of RRA as Fig. 12(c), (d), (e) and (f) show the beam steering performance in the H-plane at 122 GHz, E-plane at 122 GHz, H-plane at 128 GHz and E-plane at 128 GHz, respectively. It is visible that the maxima of the steered radiation pattern moves to a higher scanning angle for the same phase configuration at lower frequencies. For instance, phase configuration which is expected to steer the beam at 45° in E-plane at 122 GHz has the maxima at 48°. On the other hand, maxima which is expected at 45°, appears at 42° in E-plane at 128 GHz. 3D radiation patterns of beam steering angles at 122 GHz, 125 GHz and 128 GHz in E- and H-plane are shown in Fig. 13.

Furthermore, the 1-bit quantisation of unit cells also affects these results. This phenomenon usually occurs at

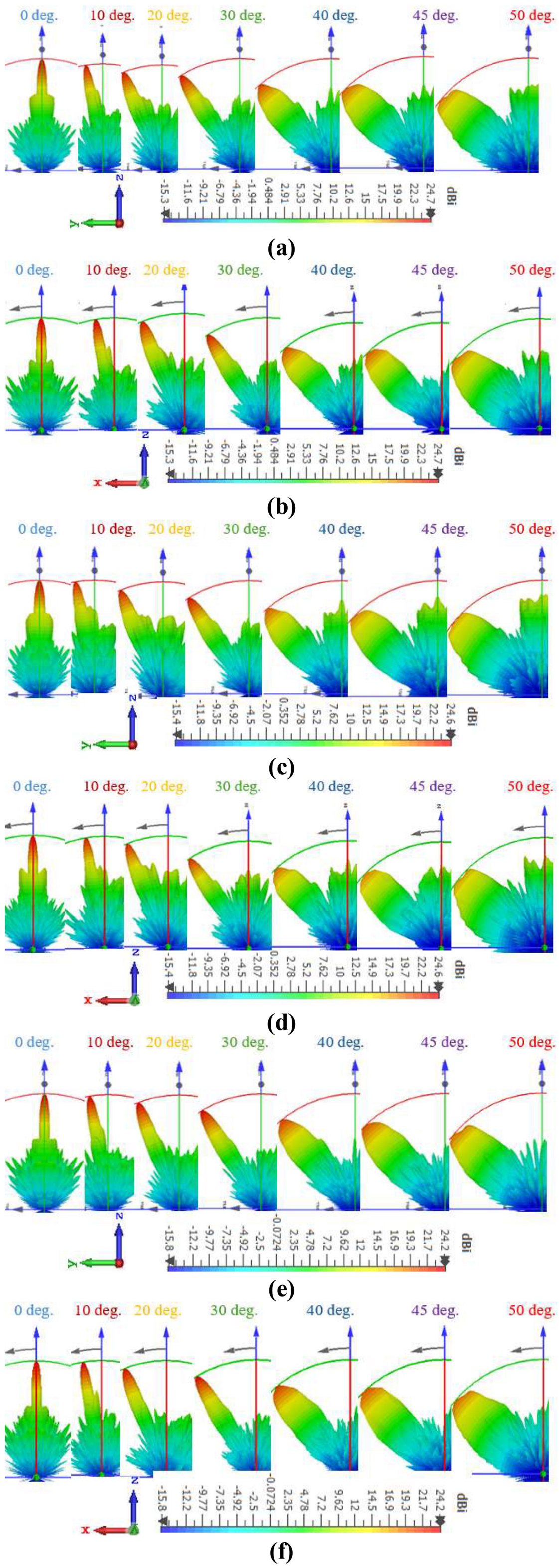

FIGURE 13. Simulated 3D radiation patterns in (a) H-plane at 125 GHz, (b) E-plane at 125 GHz, (c) H-plane at 122 GHz, (d) E-plane at 122 GHz, (e) H-plane at 128 GHz and (f) E-plane at 128 GHz.

highly steered beams, where the phase distribution of array elements changes more frequently than lesser steered angles. Moreover, these frequent changes in the required phase distribution also cause the variation in the actual reflection phase from the predicted values. It can be noticed that there is not much difference between the beam steering performance of the steered beam in the H-plane and E-plane. This is due to the almost symmetrical performance of the feed antenna. Therefore, further analysis is conducted only on E-plane.

TABLE 2. Comparison of the performance at different F/D at 125 GHz.

Theta (deg.)	Max. Gain (dBi)		SLL (dB)		-3 dB beamwidth (deg.)	
	F/D = 0.9	F/D = 1.1	F/D = 0.9	F/D = 1.1	F/D = 0.9	F/D = 1.1
0	25.6	23.3	-14.6	-15	3.9	4.1
10	24.3	22.8	-13.7	-7.4	4.1	4.2
20	24	23.2	-13.2	-15.3	5.4	5
30	23.5	23.7	-16.3	-15.6	6.4	5.4
40	20.5	21.8	-10.9	-13.2	13.2	9
45	19.3	21.2	-13.3	-12.7	17.7	11.3
50	18.2	19.8	-10.8	-11.2	19.3	16.3

Later, the effect of the F/D ratio was analysed on the collimated beam at different angles as it can assist in finding the best position to illuminate RRA for optimum beam steering performance [43], [44]. The distance between the horn antenna and the reflectarray was varied from 26.5 mm to 33.5 mm, which is also equivalent to an F/D ratio of 0.9 and 1.1 respectively. Table 2 summarises the key performance characteristics of the RRA in the case of F/D ratios of 0.9 and 1.1. It can be distinguished from the steered beams at different F/D that gain at theta, 0° increases to 25.6 dBi when the distance between feed antenna and reflectarray is decreased. In contrast, the highest gain reduces when the F/D ratio is increased. However, the decline in maximum gain in the case of F/D ratio 0.9 at up to 30° beam steering is 3 dB. With a further steered beam, the reduction in maximum gain is over 3 dB. In contrast, the gain is reduced by 2.1 dB in the case of a 1.1 F/D ratio with beam steering up to 45° as the maximum gain at 0° is 23.3 dBi and it is 21.2 at 45°. The Side Lobe Level (SLL) is below -10 dB in all cases except at a 10° steered angle in the case of F/D $= 1.1$. This is also apparent in Fig. 12(b) in the case of F/D ratio $= 1$ but it is -13.7 dB at F/D $= 0.9$. In other words, the side lobe level for a 10° steered beam can be reduced by decreasing the distance between the reflectarray plane and the phase centre of the feed antenna. This is possibly due to the radiation pattern of the feed antenna in the E-plane. It must also be recalled that the F/D ratio analyses are conducted in E-plane. In addition, -3 dB beamwidth is also smaller in the case of an F/D ratio of 1.1 than 0.9 in most of the steered radiation patterns. -3 dB beamwidth is below 10° until steering angle of 40° at F/D $= 1.1$. However, it crosses 10° when the steering angle is 40° at F/D $= 0.9$. In short, it can be concluded that the high beam steering capacity is possible at the cost of reduced maximum gain.

Fig. 14 shows the aperture efficiency of steered beams at different angles along with the quantisation efficiency. The aperture efficiency was calculated using (11) [10]:

TABLE 3. Comparison of the state-of-the-art high-frequency RRAs.

Ref.	Freq (GHz)	Tuning Method	Unit cell	Antenna size	Maximum gain (dBi)	Application	Steering range	Aperture efficiency (%)
[46]	115	LC	λ/2×λ/2	20λ×20λ×20λ	16.55	2D beam steering	20°	1
[13]	73	PIN Diode	λ/2×λ/2	8λ×8λ×18λ	16.8	2D beam steering	140°	6.2
[47]	100	LC	0.4λ×0.36λ	21λ×19λ×30λ	19.4	2D beam steering	120°	2
[48]	108	LC	0.36λ×0.36λ	7 λ×7λ×10λ	24.3	2D beam steering	80°	-
[16]	1600	Graphene	λ/16×λ/16	10λ×10λ×8λ	17.8	Vortex beams	-	6.2
[49]	390-550	Graphene	λ/2×λ/2	6.5λ×6.5λ×14λ	22.6	Frequency tuning	-	12
[45]	1600	Graphene	λ/2×λ/2	20λ×20λ×22λ	19	Single beam	-	2
This work	125	Graphene	λ/2	15λ×15λ×17λ	24.7	2D beam steering	80°	13

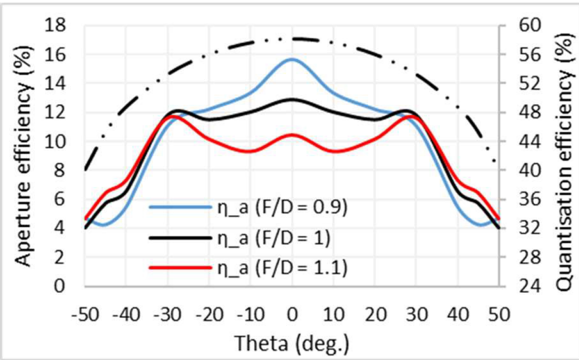

FIGURE 14. Calculated aperture efficiency (---) and quantisation efficiency (---) for different beam steering angles at 125 GHz.

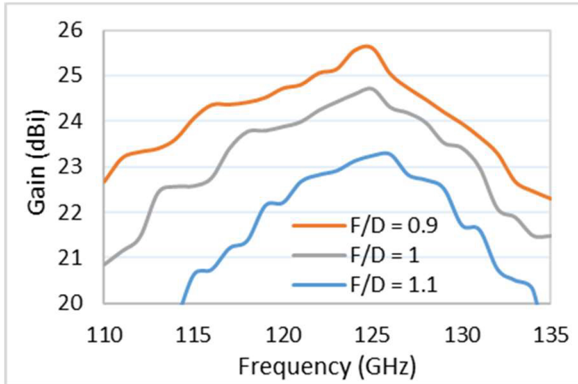

FIGURE 15. Maximum gain versus frequency for broadside radiation pattern.

$$\eta_a = \frac{G(\theta,\ \varphi)_{max}}{\frac{4\pi A_p}{\lambda^2}} \tag{11}$$

Here, η_a represents the aperture efficiency of RRA, $G(\theta, \varphi)_{max}$ represents the maximum gain obtained at an angle of (θ, φ), and A_p represents the physical aperture of the designed antenna, which is 3848 mm^2.

The maximum gain of 25.6 dBi and the aperture efficiency of 16% was obtained at 25.6 at $(\theta, \varphi) = (0, 0)$ in the case of F/D ratio 0.9. However, the maximum gain reduces drastically with increasing angle of steering Consequently that results in reduced aperture efficiency from 16% to 11% at $(\theta, \varphi) = (30, 0)$.

The quantisation loss significantly affects the aperture efficiency of highly steered beams. A reduction in quantisation efficiency is realised from 58% at an angle of 0° to 53% at 30°. Moreover, a pronounced decline is observed at a 50° steering angle, where the quantisation efficiency diminishes to 40%. This trend underscores the sensitivity of aperture efficiency to quantization effects as the beam steering angle increases, indicating that greater steering results in more pronounced losses in efficiency. In the case of F/D = 1, the aperture efficiency stays stable from the steering angle of $(\theta, \varphi) = (0, 0)$ to $(\theta, \varphi) = (30, 0)$ as there is the decline of only 2% from 13% to 11%. However, in the case of F/D = 1.1, the aperture efficiency increases with increasing from 10% at $(\theta, \varphi) = (0, 0)$ to 12% at $(\theta, \varphi) = (30, 0)$. Fig. 15 shows the maximum gain versus frequency. The 1-dB bandwidth was also confirmed to be 7.2%, 6.4% and 8.8% in the case of F/D ratio of 1, 0.9 and 1.1, respectively.

Table 3 compares the configuration and the performance parameters of the designed graphene-based RRA with state-of-the-art RRAs. Aperture efficiency, steering range and maximum gain of this study are compared. It is seen from the RRAs developed based on conventional tuning methods such as LC and PIN diode that the overall efficiency of RRA is very low. However, the proposed graphene-based RRA demonstrates very good aperture efficiency. This phenomenon arises from the role of graphene as a dedicated phase-shifting element positioned beneath the copper patch (serving as a reflective patch). The integration of graphene with copper significantly mitigates the switching losses commonly observed in traditional phase-shifting elements. The only limitation found was the limited capacity of beam steering, which is up to 45° in this work. In contrast to existing state-of-the-art graphene-based reflectarrays, the primary distinction of this study lies in the fact that the RRA elements are powered by graphene while maintaining dimensions of less than half the wavelength (λ/2). This work represents a pioneering development in which a graphene-assisted RRA has been specifically engineered for beam steering application. An RRA was proposed in [16] for the production of the vortex beams, where each unit cell was less than λ/16 dimensions. In [45], graphene was designed at $\lambda/2$ but it served its main purpose as the single beam reflectarray.

In [49], graphene-based RRA was proposed for tuning the frequency of operation. It can be seen that the model of graphene as a phase-shifting element produces great performance in terms of aperture efficiency in RRA and most importantly paving the way for beam steering at very high frequencies.

V. CONCLUSION

A graphene-based RRA has been proposed at 125 GHz frequency for point-point 6G communications. A 2D graphene sheet was embedded between the substrate and the main patch element to tune the unit cells electronically. With the application of biasing to graphene, graphene's chemical potential changes leading to the change in the reflection coefficient phase of the unit cell. An array of 977 elements was designed with the 1-bit configuration of graphene to produce a collimated beam in the desired direction. Later, the performance of RRA was invested in E-plane and H-plane. Moreover, the distance between the phase centre of the feed antenna and the array was also varied for further analysis of the designed antenna's beam steering performance. Future work includes improvisation of the required phase configuration for beam steering at an angle over 30°. The highest possible gain at large steered angles can be obtained using an empirical optimisation process to search for the best configuration.

REFERENCES

[1] Z. Xiao, Q. Yang, J. Huang, Z. Huang, W. Zhou, Y. Gao, R. Shu, and Z. He, "Terahertz communication windows and their point-to-point transmission verification," *Appl. Opt.*, vol. 57, no. 27, p. 7673, Sep. 2018, doi: 10.1364/ao.57.007673.

[2] L. Deng, Y. Zhang, J. Zhu, and C. Zhang, "Wide-band circularly polarized reflectarray using graphene-based pancharatnam-berry phase unit-cells for terahertz communication," *Materials*, vol. 11, no. 6, p. 956, 2018, doi: 10.3390/ma11060956.

[3] I. F. Akyildiz, C. Han, and S. Nie, "Combating the distance problem in the millimeter wave and terahertz frequency bands," *IEEE Commun. Mag.*, vol. 56, no. 6, pp. 102–108, Jun. 2018, doi: 10.1109/MCOM.2018.1700928.

[4] M. R. Chaharmir and J. Shaker, "Design of a broadband, dual-band, large reflectarray using multi open loop elements," in *Proc. IEEE Int. Symp. Antennas Propag.*, 2010, pp. 2875–2883, doi: 10.1109/APS.2010.5562008.

[5] E. C. Choi and S. Nam, "W-band low phase sensitivity reflectarray antennas with wideband characteristics considering the effect of angle of incidence," *IEEE Access*, vol. 8, pp. 111064–111073, 2020, doi: 10.1109/ACCESS.2020.2996707.

[6] A. Forouzmand and H. Mosallaei, "Tunable two-dimensional optical beam steering with reconfigurable indium tin oxide plasmonic reflectarray metasurface," *J. Opt.*, vol. 18, no. 12, 2016, Art. no. 125003, doi: 10.1088/2040-8978/18/12/125003.

[7] I. G. Lee, J. Y. Kim, and I. P. Hong, "Design of multi-functional transmitarray with active linear polarization conversion and beam steering capabilities," *Appl. Sci.*, vol. 12, no. 9, p. 4319, 2022, doi: 10.3390/app12094319.

[8] M. I. Abbasi, M. Y. Ismail, and M. R. Kamarudin, "Development of a pin diode-based beam-switching single-layer reflectarray antenna," *Int. J. Antennas Propag.*, vol. 2020, pp. 1–9, no. 1, 2020, doi: 10.1155/2020/8891759.

[9] X. Pan, F. Yang, S. Xu, and M. Li, "A 10 240-element reconfigurable reflectarray with fast steerable monopulse patterns," *IEEE Trans. Antennas Propag.*, vol. 69, no. 1, pp. 173–181, Jan. 2021, doi: 10.1109/TAP.2020.3008623.

[10] S. G. Lee, Y. H. Nam, Y. Kim, J. Kim, and J.-H. Lee, "A wide-angle and high-efficiency reconfigurable reflectarray antenna based on a miniaturized radiating element," *IEEE Access*, vol. 10, pp. 103223–103229, 2022, doi: 10.1109/ACCESS.2022.3204400.

[11] E. Baladi, M. Y. Xu, N. Faria, J. Nicholls, and S. V. Hum, "Dual-band circularly polarized fully reconfigurable reflectarray antenna for satellite applications in the Ku-band," *IEEE Trans. Antennas Propag.*, vol. 69, no. 12, pp. 8387–8396, Dec. 2021, doi: 10.1109/TAP.2021.3090577.

[12] W. Zhang, Y. Li, and Z. Zhang, "A reconfigurable reflectarray antenna with an 8 μm-thick layer of liquid crystal," *IEEE Trans. Antennas Propag.*, vol. 70, no. 4, pp. 2770–2778, Apr. 2022, doi: 10.1109/TAP.2021.3125378.

[13] C. Liu, F. Yang, S. Xu, and M. Li, "An E-band reconfigurable reflectarray antenna using p-i-n diodes for millimeter-wave communications," *IEEE Trans. Antennas Propag.*, vol. 71, no. 8, pp. 6924–6929, Aug. 2023, doi: 10.1109/TAP.2023.3291087.

[14] A. Campos-Jara, P. García Parejo, and A. Álvarez-Herrero, "Optimization of the response time measuring method for liquid crystal variable retarders," *J. Vac. Sci. Technol. B, Nanotechnol. Microelectron. Mater. Process. Meas. Phenom.*, vol. 37, no. 6, Nov. 2019, Art. no. 62930, doi: 10.1116/1.5122786.

[15] E. Carrasco and J. Perruisseau-Carrier, "Reflectarray antenna at terahertz using graphene," *IEEE Antennas Wireless Propag. Lett.*, vol. 12, pp. 253–256, 2013, doi: 10.1109/LAWP.2013.2247557.

[16] Z. Chang, B. You, L. S. Wu, M. Tang, Y. P. Zhang, and J. F. Mao, "A reconfigurable graphene reflectarray for generation of vortex THz waves," *IEEE Antennas Wireless Propag. Lett.*, vol. 15, pp. 1537–1540, May 2016, doi: 10.1109/LAWP.2016.2519545.

[17] Z. K. Meng, Y. Shi, W. Y. Wei, Y. Zhang, and L. Li, "Graphene-based metamaterial transmitarray antenna design for the generation of tunable orbital angular momentum vortex electromagnetic waves," *Opt. Mater. Express*, vol. 9, no. 9, p. 3709, 2019, doi: 10.1364/ome.9.003709.

[18] P. Ren, L. Jiang, and P. Li, "Graphene based tunable terahertz holographic antennas," *IEEE Open J. Antennas Propag.*, vol. 3, pp. 324–332, 2022, doi: 10.1109/OJAP.2022.3158203.

[19] E. Carrasco, M. Tamagnone, and J. Perruisseau-Carrier, "Tunable graphene reflective cells for THz reflectarrays and generalized law of reflection," *Appl. Phys. Lett.*, vol. 102, no. 10, 2013, Art. no. 104103, doi: 10.1063/1.4795787.

[20] S. Sun, W. Li, and X. Shi, "A reconfigurable graphene reflectarray for generation of OAM in thz band," in *Proc. Int. Conf. Microw. Millim. Wave Technol.*, vol. 15, 2019, pp. 1537–1540, doi: 10.1109/ICMMT45702.2019.8992481.

[21] B. Xiao, M. Gu, K. Qin, and S. Xiao, "Absorption enhancement in graphene with an efficient resonator," *Opt. Quantum Electron.*, vol. 49, no. 5, pp. 1–8, 2017, doi: 10.1007/s11082-017-1013-8.

[22] D. Correas-Serrano and J. S. Gomez-Diaz, "Graphene-based Antennas for Terahertz Systems: A Review," 2017, *arXiv:1704.00371*.

[23] A. D. Squires et al., "Electrically tuneable terahertz metasurface enabled by a graphene/gold bilayer structure," *Commun. Mater.*, vol. 3, no. 1, pp. 1–9, 2022, doi: 10.1038/s43246-022-00279-7.

[24] A. K. Worku and D. W. Ayele, "Recent advances of graphene-based materials for emerging technologies," *Results Chem.*, vol. 5, Jan. 2023, Art. no. 100971, doi: 10.1016/j.rechem.2023.100971.

[25] R. Yadav, V. S. Pandey, and P. Verma, "Nano-scaled graphene plasmonic-based vanadium dioxide Yagi-Uda array MIMO antenna for terahertz applications," *Plasmonics*, to be published, doi: 10.1007/s11468-024-02239-y.

[26] M. A. K. Khan, M. I. Ullah, R. Kabir, and M. A. Alim, "High-performance graphene patch antenna with superstrate cover for terahertz band application," *Plasmonics*, vol. 15, no. 6, pp. 1719–1727, 2020, doi: 10.1007/s11468-020-01200-z.

[27] Z. Jiao and H. J. W. Zandvliet, "Determination of the Fermi velocity of graphene on MoS2using dual mode scanning tunneling spectroscopy," *Appl. Phys. Lett.*, vol. 118, no. 16, 2021, Art no. 163103, doi: 10.1063/5.0046658.

[28] K. I. Bolotin et al., "Ultrahigh electron mobility in suspended graphene," *Solid State Commun.*, vol. 146, no. 9–10, pp. 351–355, 2008, doi: 10.1016/j.ssc.2008.02.024.
[29] T. Wang, Y. Zhang, H. Zhang, and M. Cao, "Dual-controlled switchable broadband terahertz absorber based on a graphene-vanadium dioxide metamaterial," *Opt. Mater. Express*, vol. 10, no. 2, p. 369, Feb. 2020, doi: 10.1364/OME.383008.
[30] M. R. Nickpay, M. Danaie, and A. Shahzadi, "Graphene-based metamaterial absorber for refractive index sensing applications in terahertz band," *Diam. Relat. Mater.*, vol. 130, Dec. 2022, Art. no. 109539, doi: 10.1016/j.diamond.2022.109539.
[31] N. Kiani, F. Tavakkol Hamedani, and P. Rezaei, "Switchable circular polarization in flower-shaped reconfigurable graphene-based THz microstrip patch antenna," *Analog Integr. Circuits Signal Process.*, vol. 118, no. 2, pp. 259–270, 2024, doi: 10.1007/s10470-023-02215-2.
[32] A. K. Denisultanov, S. E. Azbite, N. S. Balbekin, S. I. Gusev, and M. K. Khodzitsky, "Optical properties of graphene on quartz and polyethylene substrates in terahertz frequency range," *Proc. Prog. Electromagn. Res. Symp.*, 2015, pp. 2022–2025, 2014.
[33] E. Wang, G. Peng, K. Zhong, F. Wu, Z. H. Jiang, R. Sauleau, and W. Hong, "A 1296-cell reconfigurable reflect-array antenna with 2-bit phase resolution for Ka-band applications," *IEEE Trans. Antennas Propag.*, vol. 72, no. 4, pp. 3425–3437, Apr. 2024, doi: 10.1109/TAP.2024.3368220.
[34] B. Xi, Y. Xiao, K. Zhu, Y. Liu, H. Sun, and Z. Chen, "1-bit wideband reconfigurable reflectarray design in Ku-band," *IEEE Access*, vol. 10, pp. 4340–4348, 2022, doi: 10.1109/ACCESS.2021.3117693.
[35] M. T. Nguyen, T. T. Nguyen, and B. D. Nguyen, "Wideband transmitarray unit-cell design with 1-bit phase control and twistable polarization," *IEEE Microw. Wirel. Components Lett.*, vol. 32, no. 6, pp. 627–630, Jun. 2022, doi: 10.1109/LMWC.2022.3146022.
[36] M. Y. Ismail, M. I. Abbasi, A. F. M. Zain, M. Amin, and M. F. L. Abdullah, "Characterization of loss and bandwidth performance of reflectarray antenna based on lumped components," *Int. J. Electr. Eng. Inf.*, vol. 2, no. 2, pp. 113–122, Jun. 2010, doi: 10.15676/ijeei.2010.2.2.4.
[37] X.-B. Zhao, F. Wei, X. W. Shi, and C. Zeng, "Broadband folded reflectarray antenna using single-layer cross-polarization conversion subwavelength elements," *IEEE Antennas Wireless Propag. Lett.*, vol. 20, no. 4, pp. 612–616, Apr. 2021, doi: 10.1109/LAWP.2021.3059017.
[38] P. Nayeri, F. Yang, and A. Z. Elsherbeni, *Reflectarray Antennas: Theory, Designs, and Applications*, 1st ed. Hoboken, NJ, USA: Wiley/IEEE Press, 2018. [Online]. Available: https://ieeexplore.ieee.org/servlet/opac?bknumber=8320444
[39] M. Yi, Y. Bae, and S. Yoo, "Millimeter-wave metal reflectarray antennas with sub-wavelength holes," *Electron.*, vol. 10, no. 8, p. 945, 2021, doi: 10.3390/electronics10080945.
[40] P. Mei, S. Zhang, and G. F. Pedersen, "A low-cost, high-efficiency and full-metal reflectarray antenna with mechanically 2-D beam-steerable capabilities for 5G applications," *IEEE Trans. Antennas Propag.*, vol. 68, no. 10, pp. 6997–7006, Oct. 2020, doi: 10.1109/TAP.2020.2993077.
[41] M. H. Dahri et al., "Aspects of efficiency enhancement in reflectarrays with analytical investigation and accurate measurement," *Electronics*, vol. 9, no. 11, pp. 1–26, 2020, doi: 10.3390/electronics9111887.
[42] Z. N. Chen, D. Liu, H. Nakano, X. Qing, and T. Zwick, *Handbook of Antenna Technologies*, vols. 1–4. Singapore: Springer, 2016. doi: 10.1007/978-981-4560-44-3.
[43] M. H. Dahri, M. I. Abbasi, M. H. Jamaluddin, and M. R. Kamarudin, "A review of high gain and high efficiency reflectarrays for 5G communications," *IEEE Access*, vol. 6, pp. 5973–5985, 2018, doi: 10.1109/ACCESS.2017.2786862.
[44] K. Narayanasamy, G. N. A. Mohammed, K. Savarimuthu, R. Sivasamy, and M. Kanagasabai, "A novel Ku/K band reflectarray antenna with reduced phase slope and phase sensitivity," *Int. J. RF Microw. Comput. Eng.*, vol. 31, no. 7, 2021, Art. no. e22699, doi: 10.1002/mmce.22699.
[45] A. A. Hassan, R. R. Elsharkawy, D. A. Saleeb, E. S. M. El-Rabie, and A. S. Elkorany, "Single-beam graphene reflectarray for terahertz band communication," *Analog Integr. Circuits Signal Process.*, vol. 112, no. 3, pp. 517–525, 2022, doi: 10.1007/s10470-022-02033-y.
[46] J. Yang, P. Wang, S. Sun, Y. Li, Z. Yin, and G. Deng, "A novel electronically controlled two-dimensional terahertz beam-scanning reflectarray antenna based on liquid crystals," *Front. Phys.*, vol. 8, pp. 1–7, Oct. 2020, doi: 10.3389/fphy.2020.576045.
[47] G. Perez-Palomino et al., "Design and demonstration of an electronically scanned reflectarray antenna at 100 GHz using multiresonant cells based on liquid crystals," *IEEE Trans. Antennas Propag.*, vol. 63, no. 8, pp. 3722–3727, Aug. 2015, doi: 10.1109/TAP.2015.2434421.
[48] X. Meng, M. Nekovee, and D. Wu, "The design and analysis of electronically reconfigurable liquid crystal-based reflectarray metasurface for 6G beamforming, beamsteering, and beamsplitting," *IEEE Access*, vol. 9, pp. 155564–155575, 2021, doi: 10.1109/ACCESS.2021.3125837.
[49] S. H. Zainud-Deen, A. M. Mabrouk, and H. A. Malhat, "FFrequency tunable graphene metamaterial reflectarray," *Wireless Pers. Commun.*, vol. 103, no. 2, pp. 1849–1857, 2018, doi: 10.1049/joe.2018.5016.

SUHAIL ASGHAR QURESHI received the B.E. degree in electronics engineering from the Quaid-e-Awam University of Engineering, Science and Technology, Nawabshah, in 2018, and the master's degree in electrical engineering from the Universiti Tun Hussein Onn Malaysia, Malaysia, where he is currently pursuing the Ph.D. degree with focus on telecommunication. He has published in various WoS and Scopus indexed journals and conference proceedings. His research interests include metasurface, designing of reconfigurable reflectarray antenna, reflective intelligent surface, designing of microwave sensors, and measurement of dielectric properties of various materials. He has received multiple Gold, Silver, and Bronze awards in local and international research exhibitions.

MUHAMMAD RAMLEE KAMARUDIN (Senior Member, IEEE) received the degree (Hons.) in electrical and telecommunication engineering from Universiti Teknologi Malaysia, Johor Bahru, Malaysia, in 2003, and the M.Sc. degree in communication engineering and the Ph.D. degree in electrical engineering from the University of Birmingham, Birmingham, U.K., in 2004 and 2007, respectively, under the supervision of Emeritus Prof. P. Hall. He has been an Associate Professor with the Faculty of Electrical and Electronic Engineering, Universiti Tun Hussein Onn Malaysia (UTHM) since May 2019. Prior to this appointment, he was a Senior Lecturer with the Centre for Electronic Warfare, Information and Cyber, Cranfield Defense and Security, Cranfield University, U.K., and an Associate Professor with the Wireless Communication Centre, Universiti Teknologi Malaysia. He is currently the Deputy Director of the International Office, UTHM. His research interests include antenna design for 5G/6G, MIMO antennas, array antenna for beam-forming and beam steering, wireless on- body communications, in- body communications (implantable antenna), RF and microwave communication systems, and antenna diversity. In 2020, he received the recognition as one of the Top Research Scientists Malaysia from the Academy of Sciences Malaysia, for his achievement and contributions in this field. He is an Associate Editor of *Electronics Letters* and *IET Microwaves, Antennas and Propagation*, and an Academic Editor of the *International Journal of Antennas and Propagation*.

YOSHIHIDE YAMADA (Senior Member, IEEE) received the bachelor's and master's degrees in engineering from the Nagoya Institute of Technology in 1971 and 1973, respectively, and the Ph.D. degree in electrical engineering from the Tokyo Institute of Technology in 1989. He joined the Electrical Communication Laboratories, Nippon Telegraph and Telephone Corporation (NTT) in 1973, and moved to NTT Mobile Communications Network, Inc., (NTT DoCoMo) in 1993. In 1998, he joined National Defense Academy as a Professor. In 2014, he joined the Malaysia Japan International Institute of Technology, Universiti Teknologi MARA, Malaysia, as a Professor. His research interests include aperture antennas, array antennas, very small antennas, and radar cross sections. He received the Excellent Paper Award and the Best Tutorial Paper Award from IEICE in 2013 and 2014, respectively. He is a Fellow of IEICE Japan, a Senior Member of IEEE APS, and a member of ACES.

MUHAMMAD INAM ABBASI (Senior Member, IEEE) received the B.Sc. degree in electrical engineering with major in telecommunication from the Centre for Advanced Studies in Engineering (Islamabad), University of Engineering and Technology, Taxilla, Pakistan, in 2008, and the master's and Ph.D. degrees in electrical engineering from the Universiti Tun Hussein Onn Malaysia (UTHM) in 2011 and 2016, respectively. He joined the Wireless and Radio Science Centre (WARAS), UTHM as a Graduate Research Assistant in 2009. He was a Postdoctoral Research Fellow with the Wireless Communication Centre, Universiti Technologi Malaysia in 2017 and 2018. He is currently a Senior Lecturer with the Faculty of Electrical and Electronic Engineering Technology, Universiti Teknikal Malaysia Melaka. His recent research interests include high performance planar and printed antenna design, the study of passive and reconfigurable reflect array and planar reflector antennas, and investigation of novel materials for the design of enhanced performance antennas.

MUHAMMAD HASHIM DAHRI (Member, IEEE) received the B.E. degree in telecommunications from the Mehran University of Engineering and Technology, Pakistan, in 2010, the master's degree by research in electrical engineering from the Universiti Tun Hussein Onn Malaysia (UTHM) in 2014, and the Ph.D. degree from the Wireless Communication Centre, Univerisiti Teknologi Malaysia in 2019. He worked as a Postdoctoral Research Fellow with UTHM in 2020. He is Currently a Assistant Professor in Department of Telecommunication Engineering, Dawood University of Engineering and Technology. He has authored over 50 research articles in various indexed journals and conference proceedings. His research interests include reflectarray antennas, planar printed antennas, and tunable materials for antenna design.

ZUHAIRIAH ZAINAL ABIDIN (Senior Member, IEEE) received the Ph.D. degree from Bradford University, U.K., in 2011. She is currently the Head of the Advanced Telecommunication Research Center, Faculty of Electrical and Electronic Engineering, Universiti Tun Hussein Onn Malaysia. She has authored and co-authored several journals and proceedings. Her research interests include MIMO antenna, printed microstrip antenna, wearable antennas, metamaterial resonator, energy harvesting, electromagnetic bandgap for wireless and mobile, and high-speed digital circuit applications.

NORDIN RAMLI (Senior Member, IEEE) received the B.Eng. degree in electrical engineering from Keio University, Tokyo, Japan, in 1999, and the M.Eng. and Ph.D. degrees in electronic engineering from The University of Electro-Communications, Chofu, Japan, in 2005 and 2008, respectively. He is a Senior Staff Researcher with the Wireless Innovation Department, Corporate Technology Department, MIMOS Berhad, Kuala Lumpur. Here, he is managing the research and development work for MIMOS's in house technology development to the government and enterprise sector, especially the Internet of Things (IoT) and big data-related projects. Based on his work, he has published more than 100 journals and, conference papers, and filed more than 30 patents related to wireless communications which are pending at the World Intellectual Property Organization and Intellectual Property Corporation of Malaysia (MyIPO). On the research and development, his interests include cognitive radio, TV white space, space-time processing, equalization, adaptive array system and wireless mesh networking, IoT, and big data analytic and 5G and beyond. He is an award recipient of the Top Research Scientist Malaysia in 2018 and the Young Scientist Network by the Academy of Sciences Malaysia in 2014. He has been serving as an Associate Editor for the *IEICE Communication Express* since June 2014.